




# Efficient Computation of Radiative Heat Recovery from Porous Ceramic Monoliths for Efficient Solar Thermochemical Fuel Production

Aniket S. Patankar<sup>1</sup>, Xiao-Yu Wu<sup>2</sup>, Wonjae Choi<sup>3</sup>, Harry L. Tuller<sup>1</sup>, and Ahmed F. Ghoniem<sup>1</sup>

<sup>1</sup> Massachusetts Institute of Technology, USA

<sup>2</sup> University of Waterloo, Canada

<sup>3</sup> Ewha Womans University, South Korea

**Abstract.** Solar thermochemical hydrogen (STCH) produced by heat-driven water-splitting is a promising route for producing green hydrogen and other zero-emission synfuels. However, the efficiency of STCH must be dramatically increased for it to make an impact on decarbonization efforts. We have previously presented a novel Reactor Train System (RTS) for significantly increasing the efficiency of STCH by employing heat recovery from the redox material and efficient gas exchange processes. In this paper we present a higher-fidelity model for the RTS that accommodates the slow heat diffusion through the STCH redox material. For this purpose, a novel method is introduced for transient modelling of radiative heat in participating media. This method, called GREENER: Generalized Radiation Exchange Factors and Net Radiation, combines the accuracy of Monte Carlo Ray Tracing with the low computational cost of the P1 or Rosseland diffusion approximations. Along with STCH, GREENER has application for modelling volumetric solar receivers, high temperature heat recovery systems like heat exchangers and regenerators, and packed bed reactors. Using the GREENER method, the RTS counterflow radiative heat exchanger is shown to achieve heat recovery effectiveness greater than 70%. The performance of non-uniform porous redox morphologies is evaluated, and high-performing configurations are identified.

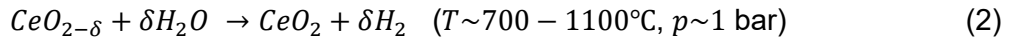
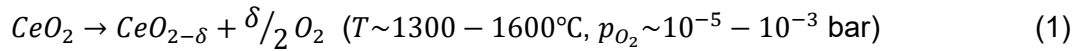
**Keywords:** Hydrogen, Solar Receiver, Monte Carlo Ray Tracing

## 1. Introduction

### 1.1 Solar Thermochemical Hydrogen (STCH) Production

STCH is a heat-driven water-splitting process, whereby a series of chemical reactions is used to split water into separate streams of oxygen and hydrogen. This work focuses on STCH using two-step redox cycles of metal oxides. The reduction and oxidation steps are shown in equations 1 and 2 respectively for ceria, the state-of-the-art STCH redox material, along with typical temperature and oxygen partial pressures conditions. Although the theoretical heat-to-fuel efficiency of STCH with ceria is over 60% [1] published demonstrations have efficiency less than 10% [2]. The two main drivers for low efficiency in demonstrated systems are (i) lack of heat recovery between the reduction and oxidation steps, (ii) Gas handling processes like oxygen removal at low partial pressure and steam-hydrogen separation. There is a trade-off between the above two drivers: higher reduction temperatures reduce the oxygen removal work, while lower oxidation temperatures reduce the hydrogen separation work. In both cases, a larger

temperature swing increases the sensible heat lost in each cycle during cool down from reduction to oxidation [3].



## 1.2 Reactor Train System (RTS)

We have previously presented a novel Reactor Train System (RTS) that overcomes the above-stated causes of inefficiency to achieve heat-to-fuel efficiency upto 40% [4], [5]. A schematic of the RTS is shown in Figure 1. The RTS has multiple ceria-containing reactors moving along a closed track. In each cycle the reactors go through 4 zones: (i) the reduction zone on the left, where reactors are heated by a radiative emitter and release oxygen; (ii) the hot section of the heat recovery zone in the middle top, where reactors transfer heat radiatively to the cold section; (iii) the oxidation zone on the right, where reactors are cooled by a radiative heat sink (to reach the target oxidation temperature) and ceria is oxidized by water to produce hydrogen; (iv) the cold section of the heat recovery zone in the middle bottom, where reactors are heated by the reactors in the hot section.

The RTS is an 'indirectly irradiated' system, where solar collection and the reactors are de-coupled. Although this necessitates more heat transfer steps, it has the advantage of enabling multi-hour storage, reduces thermal shock and allows for independent optimization of solar collection and reactors. High-temperature thermal storage (e.g. in firebrick or graphite) allows reactors to operate at high capacity factor and produce hydrogen continuously. Thermal energy from the storage is supplied to the reduction zone via the radiative emitter (Figure 1).

The base-case RTS configuration considered here has 15 reactors in each of the 4 zones, resulting in 60 reactors in total. Reactors move forward 1 station along the train, stay there for 1 minute, and then move on to the next station. This results in a cycle time of 60 minutes. The mass of ceria in each reactor is 166 kg, resulting in an effective ceria mass flowrate of 2.7 kg/s, and 107.6 kg hydrogen production per day with  $p_{O_2} \sim 10^{-4}$  bar.

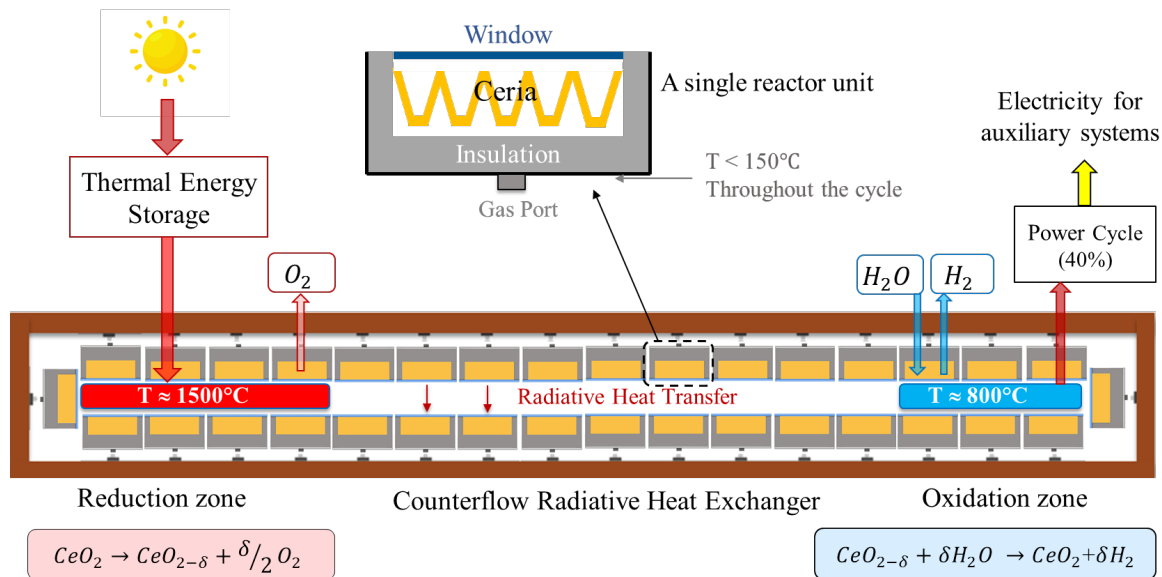


**Figure 1.** Schematic of the RTS with the redox reactions shown at the bottom. The reduction zone is supplied with solar heat at  $1500^\circ\text{C}$ , potentially with an intermediate storage unit. Waste heat from the oxidation zone heat sink can be used for electricity production to drive auxiliary systems. Schematic of a single RTS reactor is shown in the top.

### 1.3. Modelling the Reactor Train System

In our previous work modelled the RTS using a 1D model for the reactor and a lumped model for the ceria [4]. However, it has been shown that heat transfer within porous ceria is slow, and can dramatically affect the performance of the radiative heat recovery system [6]. Here we extend our previous model to include finite-rate heat transfer across the thickness of porous ceria, as shown in the new 1D model in Figure 2 left. While the model is 1D, it accounts for the differences in irradiated areas of the window, ceria cavity and insulation [3]. This work focuses on the heat transfer aspect of the RTS. Ceria is modelled as an inert material with no reduction and oxidation. While reactions and mass transfer will be taken up in future work, this work focuses on the heat recovery zone of the RTS where the enthalpy of reaction does not play a dominant role in most STCH designs.

State-of-the-art porous ceria morphologies used for STCH include reticulated porous ceramic (RPC) [7], lattices [8], [9] and other 3D ordered structures [10], as shown in Figure 2 right. We use 2 independent levers to vary porous morphology: porosity ( $\phi$ ) and cell density (or pores-per-inch  $n_{ppi}$ ). While some previous studies only used porosity to vary ceria morphology [11] Xu and Lin [10] showed that 2 independent properties can be used to tune ceria morphology. Ceria is assumed to be in the form of RPC and correlations by Ackermann et al. are used to calculate effective transport properties [12]. A constant albedo of 0.56 is considered, corresponding to partially reduced ceria [13]. Other properties of the emitter, window and insulation are the same as our previous work [3]. Ceria RPC is modelled using a volume-averaged scheme, whereby methods for radiative heat transfer in participating media are used.

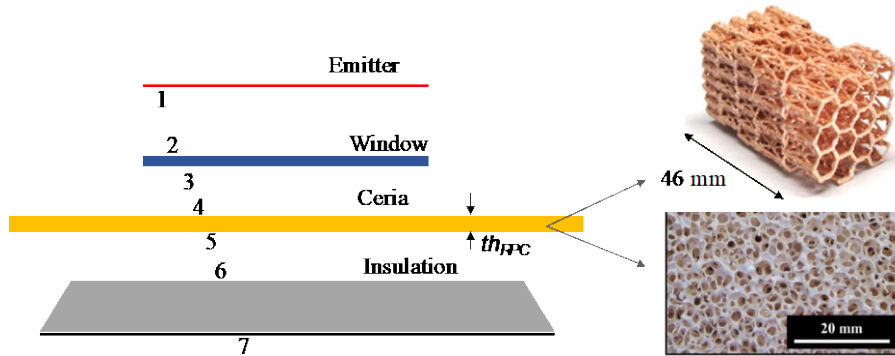


**Figure 2.** (Left) A 1D model of the RTS reactor used in this study; (Right top) A 3D printed ceria lattice [8]; (Right bottom) Ceria RPC structure [14].

## 2. The GREENER Method

We developed a novel method called 'GREENER' as part of this work for transient simulation of radiative heat transfer in participating media. GREENER stands for 'Generalized Radiation Exchange Factors and Net Radiation'. A generalized radiation exchange factor between two pieces ( $\hat{f}_{a \rightarrow b}$ ) is defined here as the fraction of radiation emitted by volume 'a' and absorbed by volume 'b'. A ray that was reflected or scattered before being absorbed by 'b' would be included in  $\hat{f}_{a \rightarrow b}$ . This is similar to the total exchange factor of F-hat factor  $\hat{F}_{a \rightarrow b}$  introduced previously for surfaces [15], [16]. In the generalized version introduced in this work, 'a' and 'b' can be volumes of a participating medium or surfaces.

### 2.1 Step 1: Pre-computation of Generalized Radiation Exchange Factors

The GREENER method proceeds in 2 steps. In the first step,  $\hat{f}_{a \rightarrow b}$  factors are calculated for the simulated geometry using (MCRT). In the RTS reactor model, the 1D ceria RPC thickness is discretized into  $N_{RPC} = 60$  isothermal elements and  $\hat{f}_{i \rightarrow j}$  is calculated between all pairs of

elements. Additionally,  $\hat{f}_{i \rightarrow 0}$  accounts for the fraction of rays emitted by element  $i$  that leave the ceria slab through the left surface. Similarly,  $\hat{f}_{i \rightarrow 61}$  accounts for radiation the ceria slab through the right surface. A sample calculation of  $\hat{f}_{10 \rightarrow j}$  is shown in Figure 3.

## 2.2 Step 2: Transient heat transfer using the Net Radiation method

Radiative heat transfer within the ceria slab is coupled with external bodies via the Net Radiation method. For the 1D reactor model showed in Figure 2, the radiative 'enclosure' consists of 6 surfaces (numbered 1-6), of which 4 surfaces (numbered 2-5) are partially transmissive, and surfaces 1 and 6 are opaque. Following Hussain and Siegel [17], the radiosity equations for surface  $i$  in this enclosure can be written as shown in equation 3. Here  $r_k$ ,  $t_k$  are reflectivity and transmissivity of surface  $k$ .  $F_{ik}$ ,  $T_{ik}$  are the classical view factor between surfaces  $i$  and  $k$  and an analogous transmission view factor respectively.  $S_i$  is the radiation emitted by surface  $i$ .

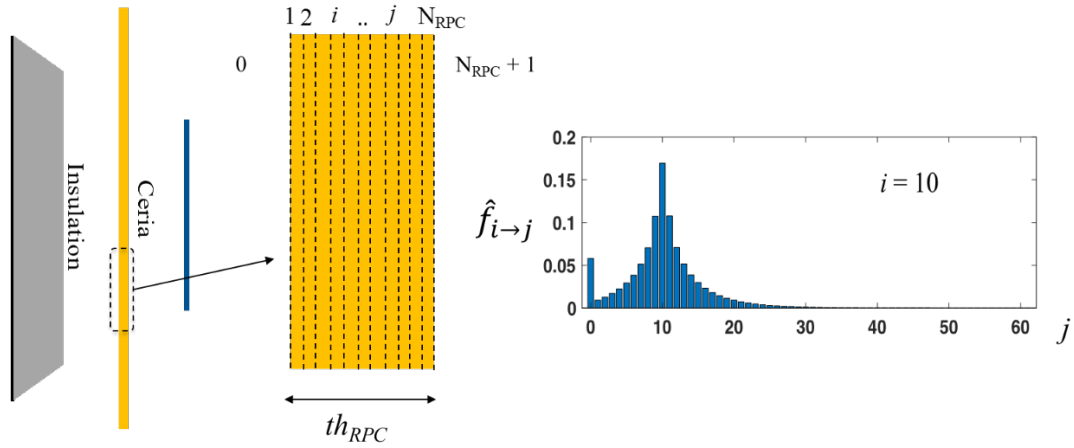


**Figure 3.** (Left) Discretization of ceria RPC thickness (Mid) A 1D ceria slab discretized along its thickness. (Right) Pre-computed  $\hat{f}_{i \rightarrow j}$  factors between ceria RPC pieces for  $i = 10$ .

As a particular example, the radiosity equation for surface 4 is shown in equation 4. Surfaces 4 and 5 have some self-irradiation because of the multicavity design shown in Figure 1. The source term sums up the radiation emitted by each piece of the RPC, where volumetric emission is considered [18] and  $\kappa_m$  is the absorption coefficient of piece  $m$  [units  $\text{m}^{-1}$ ]. Recall that  $\hat{f}_{m \rightarrow N_{RPC}+1}$  is the fraction of radiation emitted by piece  $m$  that escapes the ceria slab from surface 4. The resulting set of radiosity equations are solved to obtain the radiosity  $J$  and irradiance  $H$  of each surface. For modeling reactor-to-reactor heat transfer in the counterflow heat exchanger, a 10 surface enclosure is considered, including 2 windows and 2 RPC's and 2 bounding insulating surfaces.

$$J_i = \sum_k r_i F_{ik} J_k + S_i + \sum_k t_k T_{ik} H_k \quad (3)$$

$$J_4 = r_4 \left( \left( \frac{A_3}{A_4} \right) J_3 + r_4 \left( 1 - \frac{A_3}{A_4} \right) J_4 \right) + \sum_{m=1}^{N_{RPC}} 4\sigma \kappa_m dL T_m^4 \hat{f}_{m \rightarrow N_{RPC}+1} + t_5 \left( \left( 1 - \frac{A_6}{A_5} \right) J_5 + \frac{A_6}{A_5} J_6 \right) \quad (4)$$

Finally, the energy equation for element  $i$  of the ceria slab is shown in equation 5. The first term on the right hand side is the energy emitted by element  $j$  of the ceria slab that is absorbed by element  $i$ .  $H_4$  is the irradiance of surface 4 (Figure 2); and  $e_4$  and  $a_{4-i}$  are the effective emittance and the normalized absorption profile of surface 4. The latter 2 quantities are calculated using MCRT in the pre-computation phase. Radiation emitted by element  $i$  is subtracted out, and the last term accounts for heat conduction.

$$m_i C_p \frac{dT_i}{dt} = \sum_{j=1}^{N_{RPC}} S_j \cdot \hat{f}_{ji} + H_4 e_4 a_{4-i} + H_5 e_5 a_{5-i} - S_i + \frac{d}{dz} \left( \lambda_{effective} \frac{dT}{dz} \right) \quad (5)$$

## 2.3 Validation

The GREENER method was validated using a sample RPC-window-emitter configuration as shown in Figure 4 (left). The ceria RPC slab is insulated on the left side. The ceria and window start out cold at 800°C and the emitter is held constant at 1500°C. In this validation case the RPC has non-uniform porosity and  $n_{ppi}$  as shown in Figure 4 (left). Variation of both porosity and  $n_{ppi}$  is linear across the thickness of ceria. This particular morphology was chosen because it represents the widest possible variation of extinction coefficient ( $\beta$ ) for the range of porosities and cell densities considered in this work. The evolution of temperature profiles within the ceria RPC is shown in Figure 4 (right), comparing solutions with MCRT, GREENER and the P1 methods. Monte Carlo Ray Tracing (MCRT) is used as the gold standard to determine the accuracy of GREENER and P1. We have previously shown that the Rosseland diffusion approximation produces large errors for the present problem because of intermediate optical thickness of ceria and strongly anisotropic scattering [3]. The P1 linear anisotropic scattering coefficient is set to -1 to best match the scattering phase function given by Ackermann [12].

Temperature profiles produced by the MCRT and GREENER methods match very well, while the P1 method has noticeable deviations. Errors and computational time of the 3 methods are summarized in Table 1. This shows that the GREENER solution is within 1-2°C of the MCRT solution with a 5 order of magnitude lower computational time. The P1 temperature profile has significant errors. We also report the relative error in equilibrium oxygen non-stoichiometry of ceria ( $\delta$ ) corresponding to the temperature profiles in Figure 4 at oxygen partial pressure of  $p_{O_2} = 10$  Pa. It can be seen that relatively small errors in the P1 temperature profiles result in unacceptably high errors in the extent of reduction ( $\delta$ ). The latter corresponds to the amount of hydrogen produced in each cycle, which is a critical quantity in STCH systems.

**Table 1.** Errors in temperature profile and ceria  $\delta$ , along with computation time.

Method	Mean absolute T-error	Max T-error	Relative error in $\delta$	Computation time
MCRT	0.0°C (reference)	0.0°C (ref.)	0.00% (ref.)	$\sim 10^5$ s
GREENER	0.44°C	1.25°C	0.50%	0.83 s
P1	14.28°C	28.29°C	28.8%	1.098 s

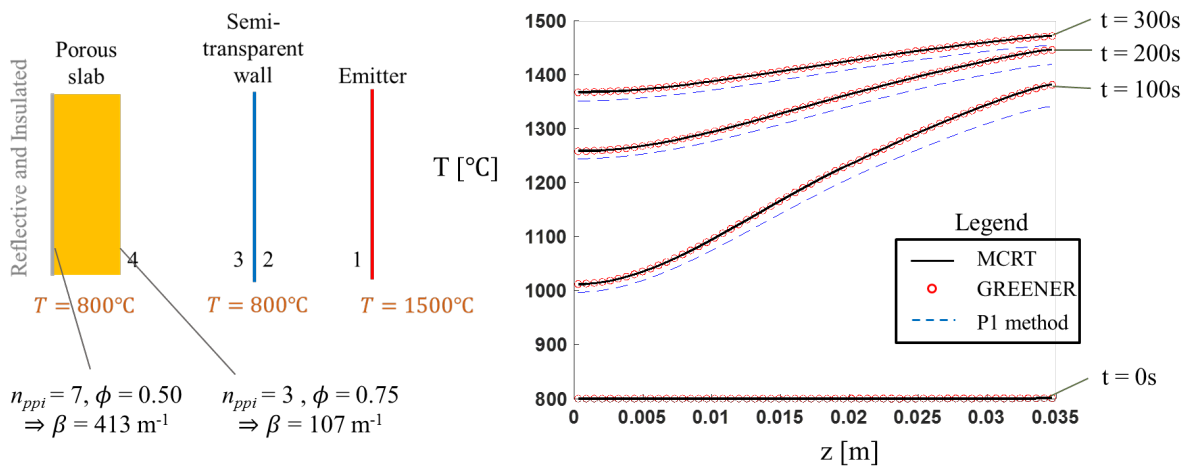


**Figure 4.** (Left) Validation geometry; (Right) Calculated temperature profiles.

### 3. Results

The GREENER method was applied to the RTS to evaluate the heat recovery effectiveness ( $\eta_{Hx}$ ) of the counterflow radiative heat exchanger, as defined in equation 6 using average ceria RPC temperatures. The RTS was simulated for 10 consecutive cycles till a periodic steady state was reached. Figure 5 left shows the average temperature of ceria RPC in each of the 60 RTS reactor stations. Reactor positions are shown in Figure 5 right-top, and some of them are marked on the temperature profiles on the left. Reactors H1-H15 and C1-C15 follow the expected counterflow heat exchanger temperature profiles. The base case ceria morphology with uniform porosity of 0.75 and  $n_{ppi} = 7$  has  $\eta_{Hx} = 65.2\%$ . The 15 hot reactor stations in the heat recovery zone (H1-H15) together transfer 7.3 kW heat to reactors C1-C15, while the heat transferred by the heat source to reactors in the reduction (R1-R15) is only 4.2 kW.

$$\eta_{Hx} = \frac{\langle T_{RPC} \rangle_{C1} - \langle T_{RPC} \rangle_{O15}}{\langle T_{RPC} \rangle_{R15} - \langle T_{RPC} \rangle_{O15}} \quad (6)$$

The ceria RPC morphology was varied while keeping the total mass of ceria in each reactor and other RTS parameters constant. This includes non-uniform morphologies, where  $n_{ppi}$  or porosity vary linearly between the 'front' and 'back' surfaces of the ceria RPC as defined in Figure 5 bottom right. These morphologies, the corresponding  $\beta$ , and the resulting  $\eta_{Hx}$  are documented in Table 2. Also shown is the maximum temperature difference between the front and back of the ceria RPC during a cycle ( $\Delta T_{f-b}$ ). Low values of  $\Delta T_{f-b}$  are preferred because they indicate lower temperature gradients and thermal stress. Case 1 shows the base morphology which was used in section 3.1. In case 2,  $n_{ppi}$  is reduced to 3 pores per inch, which reduces  $\beta$ , resulting in faster heat transfer within the ceria RPC. This significantly increases  $\eta_{Hx}$  to 71.4% and halves  $\Delta T_{f-b}$ . In the limit of infinitely fast heat transfer within the ceria RPC, i.e., uniform ceria temperature, the RTS base configuration achieves  $\eta_{Hx} = 75.5\%$  (case 7).

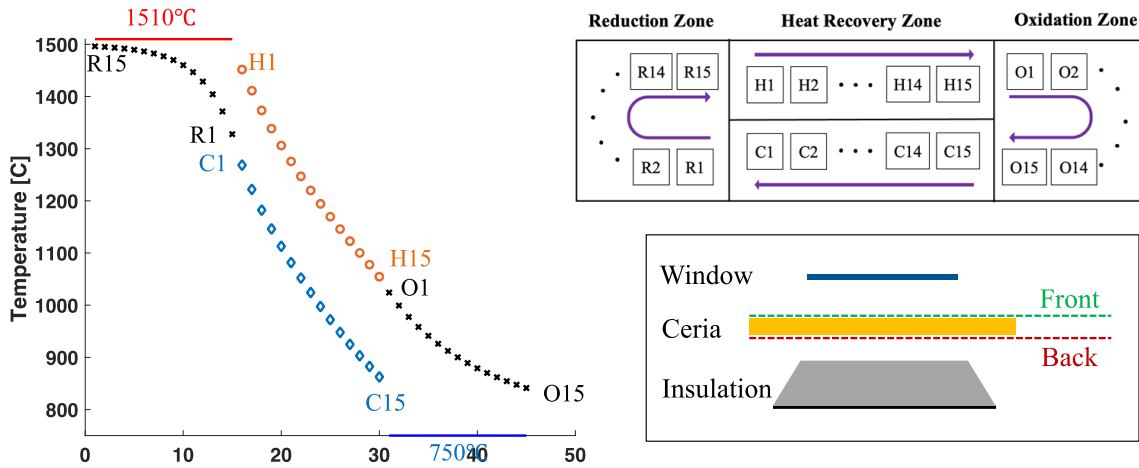


**Figure 5.** (Left) Average ceria RPC temperatures in each of the 60 reactors with the base case RPC morphology. (Right top) Schematic of RTS showing reactor positions. (Right bottom) Schematic of the 1D reactor model with the 'front' and 'back' RPC surfaces marked.

**Table 2.** Effect of ceria RPC morphology on heat recovery and temperature gradients.

Case	RPC morphology: back $\rightarrow$ front	Extinction coefficient ( $\beta$ ): back $\rightarrow$ front	$\eta_{Hx}$	$\Delta T_{f-b}$
1 (Base case)	$n_{ppi}: 7 \rightarrow 7$ $\phi = 0.75 \rightarrow 0.75$	$\beta : 325 \text{ m}^{-1} \rightarrow 325 \text{ m}^{-1}$	65.2%	158°C
2	$n_{ppi}: 3 \rightarrow 3$ $\phi = 0.75 \rightarrow 0.75$	$\beta : 139 \text{ m}^{-1} \rightarrow 139 \text{ m}^{-1}$	71.4%	81°C
3	$n_{ppi}: 7 \rightarrow 3$	$\beta : 325 \text{ m}^{-1} \rightarrow 139 \text{ m}^{-1}$	69.9%	111°C

	$\phi = 0.75 \rightarrow 0.75$			
4	$n_{ppi}: 3 \rightarrow 7$ $\phi = 0.75 \rightarrow 0.75$	$\beta : 139 \text{ m}^{-1} \rightarrow 325 \text{ m}^{-1}$	66.4%	135°C
5	$n_{ppi}: 7 \rightarrow 7$ $\phi = 0.67 \rightarrow 0.83$	$\beta : 413 \text{ m}^{-1} \rightarrow 250 \text{ m}^{-1}$	64.4%	129°C
6	$n_{ppi}: 7 \rightarrow 7$ $\phi = 0.83 \rightarrow 0.67$	$\beta : 250 \text{ m}^{-1} \rightarrow 413 \text{ m}^{-1}$	65.9%	154°C
7	Lumped Assumption	Ceria RPC has uniform T	75.5%	0°C

Cases 3 and 4 have uniform porosity and a linear variation of  $n_{ppi}$  from front to back. Case 3 has high  $n_{ppi}$  at the back, and therefore high  $\beta$ , and lower values at the front of the RPC. This results in a significant increase in  $\eta_{Hx}$  compared to the base case, but still marginally lower than case 2, which has  $n_{ppi} = 3$  throughout the RPC thickness. Case 4 is the other way around, with  $n_{ppi}$  and  $\beta$  increasing from back to front. In this case  $\eta_{Hx}$  is much lower than case 3, although still marginally higher than the base case. This shows that low  $n_{ppi}$  results in higher heat recovery. Moreover, it is better to have low  $n_{ppi}$  in front and higher in the back than the other way around, while a uniformly low  $n_{ppi}$  has the best performance. Cases 5 and 6 have uniform  $n_{ppi}$  and a linear variation of porosity from front to back. Both cases have the same average porosity that is equal to the base case porosity. Case 5 has higher porosity in the front, and therefore low  $\beta$ , while case 6 is the other way around. Interestingly, case 6 has higher  $\eta_{Hx}$  than both case 5 and the base case despite having higher  $\beta$  in the front. This differs from the trend between cases 3 and 4 where  $n_{ppi}$  was varied and porosity was constant. We explain this by noting that changing porosity does more than change  $\beta$ , it also changes mass of ceria. Case 6 has a greater fraction of ceria mass located closer to the front surface, putting it is closer to the heat source or sink, where it heats up and cools down faster. This effect seems to overpower the impact of higher  $\beta$ , although the overall impact on  $\eta_{Hx}$  is less than 1 %-point.

In summary, the best performing RPC of a given average porosity and linear morphology variations has low  $n_{ppi}$  throughout the thickness, and porosity decreasing from back to front. This might appear to contradict previous studies on directly irradiated STCH volumetric absorbers. Some STCH absorber designs use higher  $n_{ppi}$  in the back for complete attenuation of incoming solar flux (like case 3) [8], [9], [19]. On the other hand, Dai and Haussener report that RPC with low porosity in the middle and high porosity in the front and back results in the best STCH performance by reducing re-radiation losses from the back of the RPC [11]. Our findings are different, in part because the RTS reactor is heated by a hot emitter and not directly irradiated with concentrated solar flux. Moreover, we include the reactor insulation in our model, so that radiation escaping from the back of the RPC is largely reflected back by the insulation. Since thermal diffusivity in the insulation is low, the top layer heats up quickly and starts radiating back to the RPC. Thus, heat loss from the back of the RPC is relatively small. Our findings are broadly applicable to indirectly irradiated reactors with negligible reradiation losses to ambient. Directly irradiated systems like volumetric solar receivers are the subject of an ongoing study.

## 4. Conclusion

In this work we present a novel method called GREENER for transient modelling of radiative heat in participating media. This method was shown to have the same accuracy as Monte Carlo Ray Tracing, with errors of the order of 1°C. On the other hand, GREENER computational cost is several orders of magnitude lower than MCRT, and comparable to the P1 or Rosseland diffusion approximations. The GREENER method was applied to the novel Reactor Train System for thermochemical hydrogen production. The counterflow radiative heat exchanger was shown to achieve heat recovery effectiveness greater than 70%. A longer cycle time can achieve higher heat recovery at the expense of lower hydrogen production rate. Ceria foams with low cell density and lower porosity on the irradiated side have the best performance. A

comprehensive study to maximize both ceria mass loading and heat transfer rates in RTS reactors is ongoing, considering porous morphology, 3D reactor design and cycle time.

## Data availability statement

Data will be made available upon request.

## Author contributions

ASP: Conceptualization, investigation, manuscript writing; XW and WC: Review and discussion; HLT: Materials; AFG: Supervision, funding acquisition, manuscript review.

## Competing interests

The authors declare that they have no competing interests.

## Funding

Centers for Mechanical Engineering Research and Education at MIT and SUSTech.

## References

- [1] Moretti, C., Patil, V., Falter, C., Geissbühler, L., Patt, A., and Steinfeld, A., 2023, "Technical, Economic and Environmental Analysis of Solar Thermochemical Production of Drop-in Fuels," *Sci. Total Environ.*, **901**(July), p. 166005. <https://doi.org/10.1016/j.scitotenv.2023.166005>.
- [2] Zoller, S., Koepf, E., Steinfeld, A., Zoller, S., Koepf, E., Nizamian, D., Stephan, M., Patane, A., Haueter, P., and Romero, M., 2022, "A Solar Tower Fuel Plant for the Thermochemical Production of Kerosene from H<sub>2</sub>O and CO<sub>2</sub>," *Joule*, 6(7) pp. 1606–1616. <https://doi.org/10.1016/j.joule.2022.06.012>
- [3] Patankar, A. S., 2023, "System and Reactor Design, and Materials Testing for Efficient Thermochemical Solar Fuel Production in Temperature / Pressure Swing Redox Cycles," PhD thesis, Massachusetts Inst. Technol.
- [4] Patankar, A. S., Wu, X. Y., Choi, W., Tuller, H. L., and Ghoniem, A. F., 2022, "A Reactor Train System for Efficient Solar Thermochemical Fuel Production," *ASME J. Sol. Energy Eng.*
- [5] Patankar, A. S., Wu, X. Y., Choi, W., Tuller, H. L., and Ghoniem, A. F., 2022, "Efficient Solar Thermochemical Hydrogen Production in a Reactor Train System With Thermochemical Oxygen Removal," *ASME Int. Mech. Eng. Congr. Expo. Proc.*, **6**. <https://doi.org/10.1115/IMECE2022-94821>.
- [6] Falter, C. P., and Pitz-Paal, R., 2017, "A Generic Solar-Thermochemical Reactor Model with Internal Heat Diffusion for Counter-Flow Solid Heat Exchange," *Sol. Energy*, **144**, pp. 569–579. <https://doi.org/10.1016/j.solener.2017.01.063>.
- [7] Furler, P., Scheffe, J., Marxer, D., Gorbar, M., Bonk, A., Vogt, U., and Steinfeld, A., 2014, "Thermochemical CO<sub>2</sub> Splitting via Redox Cycling of Ceria Reticulated Foam Structures with Dual-Scale Porosities," *Phys. Chem. Chem. Phys.*, **16**(22), pp. 10503–10511. <https://doi.org/10.1039/c4cp01172d>.



- [8] Hoes, M., Ackermann, S., Theiler, D., Furler, P., and Steinfeld, A., 2019, "Additive-Manufactured Ordered Porous Structures Made of Ceria for Concentrating Solar Applications," *Energy Technol.*, **7**(9). <https://doi.org/10.1002/ente.201900484>.
- [9] Sas Brunser, S., Bargardi, F. L., Libanori, R., Kaufmann, N., Braun, H., Steinfeld, A., and Studart, A. R., 2023, "Solar-Driven Redox Splitting of CO<sub>2</sub> Using 3D-Printed Hierarchically Channeled Ceria Structures," *Adv. Mater. Interfaces*, **2300452**. <https://doi.org/10.1002/admi.202300452>.
- [10] Xu, D., and Lin, M., 2023, "Design Controllable TPMS Structures for Solar Thermal Applications: A Pore-Scale vs. Volume-Averaged Modeling Approach," *Int. J. Heat Mass Transf.*, **201**. <https://doi.org/10.1016/j.ijheatmasstransfer.2022.123625>.
- [11] Dai, X., and Haussener, S., 2022, "Non-Uniform Porous Structures and Cycling Control for Optimized Fixed-Bed Solar Thermochemical Water Splitting," *J. Sol. Energy Eng.*, **144**(3). <https://doi.org/10.1115/1.4052960>.
- [12] Ackermann, S., Takacs, M., Scheffe, J., and Steinfeld, A., 2017, "Reticulated Porous Ceria Undergoing Thermochemical Reduction with High-Flux Irradiation," *Int. J. Heat Mass Transf.*, **107**, pp. 439–449. <https://doi.org/10.1016/j.ijheatmasstransfer.2016.11.032>.
- [13] Ackermann, S., and Steinfeld, A., 2017, "Spectral Hemispherical Reflectivity of Nonstoichiometric Cerium Dioxide," *Sol. Energy Mater. Sol. Cells*, **159**, pp. 167–171. <https://doi.org/10.1016/j.solmat.2016.08.036>.
- [14] Zoller, S., 2020, "A 50 KW Solar Thermochemical Reactor for Syngas Production Utilizing Porous Ceria Structures," ETH Zurich.
- [15] Gebhart, B., 1957, *Unified Treatment for Thermal Radiation Transfer Processes: Gray, Diffuse Radiators and Absorbers*, The American Society of Mechanical Engineers.
- [16] Beckman W A, 1971, "Solution of Heat Transfer Problems on a Digital Computer," *Sol. Energy*, **13**, pp. 293–300.
- [17] Hussain, N., and Siegel, R., 1975, "Radiation Exchange for a System with Partially Transmitting Wall," **2**, pp. 105–114.
- [18] Modest, M. F., 2013, *Radiative Heat Transfer, 3rd Ed.*, Elsevier Inc. <https://doi.org/10.1016/C2010-0-65874-3>.
- [19] Haeussler, A., Abanades, S., Julbe, A., Jouannaux, J., and Cartoixa, B., 2020, "Solar Thermochemical Fuel Production from H<sub>2</sub>O and CO<sub>2</sub> Splitting via Two-Step Redox Cycling of Reticulated Porous Ceria Structures Integrated in a Monolithic Cavity-Type Reactor," *Energy*, **201**. <https://doi.org/10.1016/j.energy.2020.117649>.